minerals

MDPI

*Article*

# Boron Impurity Deposition on a Si(100) Surface in a $SiHCl_3$-$BCl_3$-$H_2$ System for Electronic-Grade Polysilicon Production

**Qinghong Yang [1,2,†], Fengyang Chen [1,2,†], Lin Tian [3], Jianguo Wang [4,†], Ni Yang [1,3,*], Yanqing Hou [1,*], Lingyun Huang [1,*] and Gang Xie [2,3]**

[1] State Key Laboratory of Complex Nonferrous Metal Resources Clean Utilization, Kunming University of Science and Technology, Kunming 650093, China; 20192102032@stu.kust.edu.cn (Q.Y.); fychen@stu.kust.edu.cn (F.C.)
[2] Faculty of Metallurgical and Energy Engineering, Kunming University of Science and Technology, Kunming 650093, China; wqs@stu.kust.edu.cn
[3] State Key Laboratory of Pressure Hydrometallurgical Technology of Associated Nonferrous Metal Resources, Yuantong North Road 86, Kunming 650031, China; ltian@stu.kust.edu.cn
[4] China Copper Co., Ltd., Yuantong North Road 86, Kunming 650031, China; jgwang@stu.kust.edu.cn
* Correspondence: yqh@stu.kust.edu.cn (N.Y.); hyqsimu@kust.edu.cn (Y.H.); hly@kust.edu.cn (L.H.)
† These authors contributed equally to this work.

**Abstract:** A study of boron impurities deposited on a Si(100) surface in a $SiHCl_3$-$BCl_3$-$H_2$ system is reported in this paper, using periodic density functional theory with generalized gradient approximation (GGA). The results show that the discrete distances of $BCl_3$ and $SiHCl_3$ from the surface of the Si(100) unit cell are 1.873 Å and 2.340 Å, respectively, and the separation energies are −35.2549 kcal/mol and −10.64 kcal/mol, respectively. $BCl_3$ and $SiHCl_3$ are mainly adsorbed on the surface of the Si(100) unit cell in particular molecular orientations: the positive position and the hydrogen bottom-two-front position from the analysis of the bond length change and adsorption energy. The adsorption of $SiHCl_3$ and $BCl_3$ is accompanied by a charge transfer from the molecule to the surface of the unit cell of 0.24 and 0.29 eV, respectively. $BCl_3$ reacts more readily than $SiHCl_3$ with the Si(100) surface, resulting in the deposition of boron impurities on the polysilicon surface.

**Keywords:** electronic-grade polysilicon; boron impurities; chemical vapor deposition; density functional theory; differential charge density

**Citation:** Yang, Q.; Chen, F.; Tian, L.; Wang, J.; Yang, N.; Hou, Y.; Huang, L.; Xie, G. Boron Impurity Deposition on a Si(100) Surface in a $SiHCl_3$-$BCl_3$-$H_2$ System for Electronic-Grade Polysilicon Production. *Minerals* **2022**, *12*, 651. https://doi.org/10.3390/min12050651

Academic Editors: Kenneth N. Han, Shuai Wang, Xingjie Wang and Jia Yang

Received: 12 April 2022
Accepted: 12 May 2022
Published: 21 May 2022

**Publisher's Note:** MDPI stays neutral with regard to jurisdictional claims in published maps and institutional affiliations.

**Copyright:** © 2022 by the authors. Licensee MDPI, Basel, Switzerland. This article is an open access article distributed under the terms and conditions of the Creative Commons Attribution (CC BY) license (https://creativecommons.org/licenses/by/4.0/).

## 1. Introduction

With the rapid development of the electronic information industry, silicon is a very important raw material for semiconductor manufacture, and electronic-grade polysilicon materials play a pivotal role [1,2]. Polysilicon has a high mobility in semiconductor circuits, and consequently it is widely used in such industries as semiconductors, integrated circuits and computer chips [3,4]. The polysilicon materials used in the semiconductor and electronic information industries are electronic-grade polysilicon, and are generally 99.9999% pure Si [5]. For a long time, the production technology for electronic-grade polysilicon has been monopolized by many countries. The demand for electronic-grade polysilicon in China is almost entirely dependent on imports, which are highly dependent on the international environment [6]. Because of my country's insufficient research on semiconductor materials, the purity of polysilicon has never reached the international level, and the lack of sufficiently pure silicon has become a key factor that directly hinders the development of my country's semiconductor industry.

The main processes for the production of polysilicon include chemical vapor methods and metallurgy [7]. The representative of the chemical vapor deposition methods are the modified Siemens method [8], and the fluidized-bed [9], silane [10] and gas-liquid-deposition methods [11]. The main metallurgical methods are the thermite reduction

method and the regional hot-melt purification method, but the thermite reduction method is only suitable for use in a laboratory [12,13]. Since the development of the improved Siemens chemical vapor deposition method, no other method can produce the same purity in the product and the process [14], and hence this is currently the method mainly used in industry to produce polysilicon. However, there is an unavoidable problem in production by the improved Siemens method: distilled trichlorosilane ($SiHCl_3$) and a small amount of boron trichloride ($BCl_3$) enter the Siemens reduction furnace, causing a heterogeneous reaction on the surface of the silicon rod, which results in the doping of boron into the polysilicon [15]. However, research on boron impurities arising in the production of polysilicon by the improved Siemens method is still relatively weak, and research on this process is therefore of great significance.

The impurities in high-purity electronic-grade polysilicon come mainly from the boron impurity in the acceptor, and the content of this needs to be controlled below 0.33 ppb [15]. To control the B doping of polysilicon in chemical vapor deposition, it is important to reduce the content of impurity B in the product and improve its purity [16,17], and this requires in-depth and systematic research on B-doping in the polysilicon deposition process. To study the chemical vapor deposition rate, Jenkinson and Pollard experimented to explore the deposition rate of boron in a $BCl_3$-$H_2$ system in a parallel flow reactor [18]. However, under these conditions, the boron deposition rate was limited by the transfer process of $BCl_3$. To describe the kinetics and reaction mechanism of the $BCl_3$ hydrogenation process more accurately, Sezgi designed a collision-jet chemical vapor deposition reactor [19]. The role of the reactor was to minimize the impact of the transfer process on the boron deposition rate. On this basis, Sezgi further studied the kinetics of the process of boron chemical vapor deposition in the $BCl_3$-$H_2$ system and obtained a deposition rate of B in the range of 75–1350 °C [20]. The Key Laboratory of Ultra-High Temperature Structural Composites of Northwestern Polytechnical University studied the influence of temperature on the kinetics of chemical vapor deposition during the preparation of Si-B-C ceramics. The results showed that the process is controlled by chemical reaction kinetics with an activation energy of 271 kJ/mol, the initial step of the deposition kinetics being $BCl_3$ (g) + $H_2$ (g) $\rightarrow$ $HBCl_2$ (g) + HCl (g) [21]. That study also proved that this step is one of the main reactions in the thermodynamic analysis of $ZrB_2$ synthesized using the $ZrCl_4$-$BCl_3$-$H_2$ system [22].

The doping mechanism of B in polysilicon chemical vapor deposition has been studied both domestically and abroad. To accurately and economically reflect the actual industrial situation, this study uses the method of simulation by quantum chemistry calculation to study the B-doping control mechanism in the process of polysilicon chemical gas deposition in a vacuum environment. The properties of different atomic positions of $BCl_3$ and $SiHCl_3$ on the Si(100) surface are calculated and analyzed using the first-principles method, and the most favorable state is determined by comparing the different adsorption energies. At the same time, the optimal adsorption density of states is calculated and the adsorption reaction mechanism is obtained.

## 2. Calculational Methods

On the basis of functional theory, the plane-wave method employing a supersoft pseudopotential was adopted, and a GGA-BLYP functional (a Becke–Lee–Yang–Parr functional incorporating the generalized gradient approximation) was used for the approximate calculation [23]. The DMol$^3$ module [24] in the Material Studio software package (Version 8.0, Accelrys Company, San Diego, CA, America) was used for the calculation of the gas-phase reaction, which includes the optimization of the $SiHCl_3$, $BCl_3$ and $H_2$ molecules and the calculation of the energy and frequency. The CASTEP (Cambridge Serial Total Energy Package) module [25] was used to calculate the gas–solid reaction, involving mainly the calculation of the relevant parameters of the adsorption reaction of the adsorbed molecules on the surface of the basic model and a search for the transition state of the entire adsorption reaction. For the Si(100) surface, a 7-layer structure was adopted, with the cutoff energy

selected as 450 eV and the k-point grid set to $3 \times 3 \times 1$ [26]. In the supersoft pseudopotential method, the convergence criteria of the pseudopotential have to be selected [27]. The convergence criteria for energy, force and maximum displacement are selected at the same time, with values chosen as energy ($2 \times 10^{-5}$ eV/atom), force (0.05 eV/Å) and maximum displacement ($2 \times 10^{-3}$ Å). The internal stress between atoms must be less than 0.1 GPa [28]. The path of the Brillouin zone was set to GFQZG, the complete LST/QST method was adopted for the transition state search, and a vacuum layer with a thickness of 12 Å was selected to eliminate interaction between the layers. The error in the surface energy was limited to 0.05 J/m$^2$. The formula used to calculate the surface energy is shown in Equation (1) [29]:

$$\sigma = \frac{E_{slab} - nE_{bulk}}{2A} \quad (1)$$

where $E_{slab}$ is the total energy of the unit-cell of the model, $E_{bulk}$ is the energy of a single atom in the unit cell, $n$ is the number of atoms in the unit cell, and $A$ is the total surface area of the unit cell.

The mechanism of $SiHCl_3$ decomposition on the low index plane of the polycrystal silicon is performed the same as silicon [30]. Therefore, the adsorption energy (the change in the total energy before and after adsorption) of the $SiHCl_3$ and $BCl_3$ molecules on the surface of the Si(100) unit cell is calculated using Equation (2) [31]:

$$E_{adsorption} = E_{surface^*} - E_{surface} - E_{molecules} \quad (2)$$

where $E_{adsorption}$ represents the adsorption energy of $BCl_3$ or $SiHCl_3$ onto the surface of the Si(100) unit cell, $E_{surface^*}$ represents the energy of the adsorption base surface, $E_{surface}$ is the energy of the surface without any interactions, and the total energy of the molecules before adsorption is represented by $E_{molecules}$.

Figure 1a shows the geometric structure of the model Si(100) unit cell. Its surface contains three types of Si atoms: top, bridge and acupoint Si atoms. To study the adsorption of related molecules on the polysilicon (100) surface, a complete unit cell surface must first be established. The thickness of the vacuum layer was set to 12 Å to avoid layer-to-layer interactions. In the process of establishing the model, in order to satisfy the stability of the model and the accuracy of the experiment at the same time, we did not impose any restrictions on the upper three layers of atoms but fixed the lower four layers of atoms. Simultaneously, to saturate the covalent bonds of each silicon atom in the bottom layer, two H atoms were added to each Si atom in the bottom layer, adding hydrogen atom at the bottom can increase the stability of the model, and the silica–hydrogen bond at the bottom is conducive to the stable convergence of the model, and the surface and near-surface layer atoms were fully relaxed. The supercell chemical formula for the entire unit cell is $Si_{83}H_9$. After surface optimization, the optimization curve finally reached a stable convergence state, as shown in Figure 1b, which proved that the surface structure met the experimental requirements.

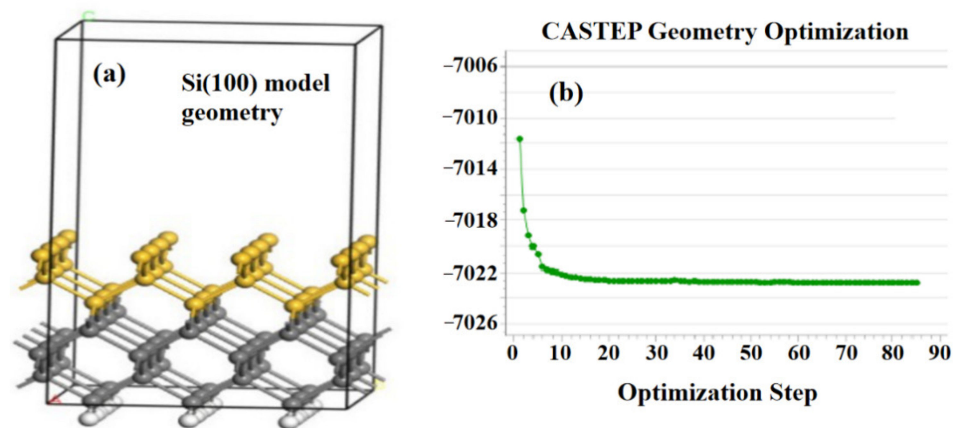


**Figure 1.** Model geometry and optimization curve of Si(100) surface. (**a**) is the Si(100) model geometry; (**b**) is the model optimization convergence curve.

## 3. Results and Discussion

### *3.1. Adsorption of $BCl_3$ on the Surface of Polysilicon Si(100)*

The molecular structure of $BCl_3$ is a plane regular triangle. The structure of $BCl_3$ adsorbed on the Si(100) surface was obtained by placing $BCl_3$ molecules on a super cell (3 × 3) surface and fully relaxing it. The surface optimization of $BCl_3$ with different structures was performed as follows. A $BCl_3$ molecule was used to establish stable adsorption models for three orientations: the side position, lateral position and positive position of the molecule. The changes in the distance before and after adsorption were compared and analyzed. The results are shown in Figure 2.

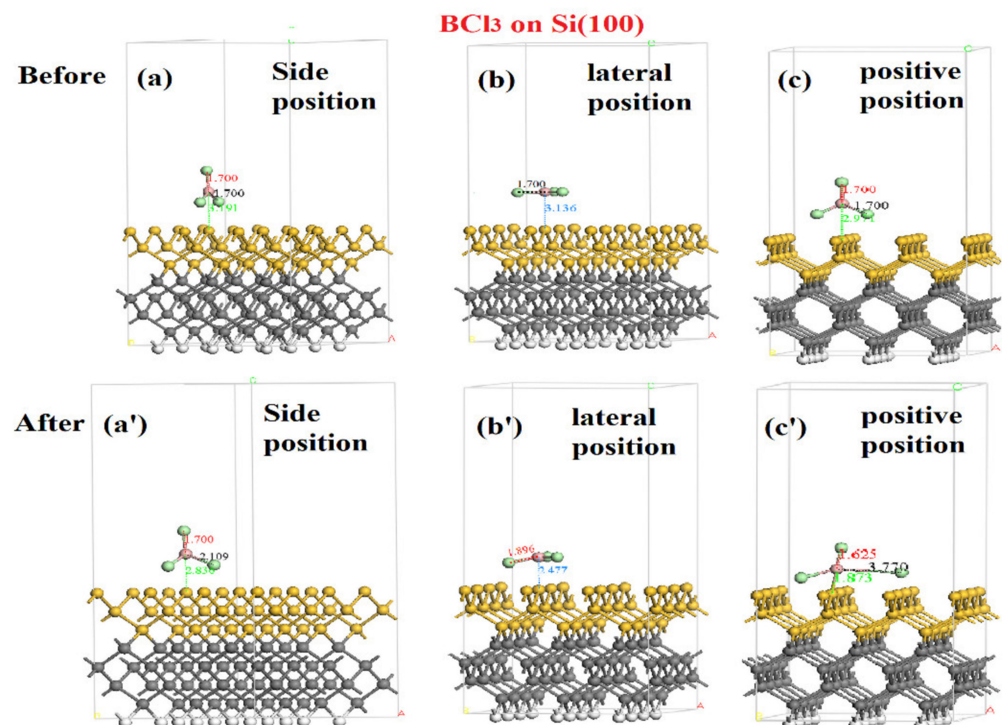


**Figure 2.** Diagrams of the molecular structure and distance of $BCl_3$ before and after adsorption on the Si(100) surface. Diagrams (**a**–**c**) show the adsorption structure before reaction, (**a′**–**c′**) the adsorption structure after the reaction, ((**a**,**a′**) show side position of the molecule, (**b**,**b′**), lateral position of the molecule, and (**c**,**c′**) positive position of the molecule).

Changes in the distance between the molecules and the surface before and after the reaction for the three adsorption structures were observed. It was found that when $BCl_3$ molecules are adsorbed on the Si(100) surface of the unit cell in the three possible structures, the distance before and after the adsorption has changed correspondingly, and the distance between the molecules and the surface of the unit cell in the three structural configurations is correspondingly shortened. This shows that an adsorption reaction between the $BCl_3$ molecule and the Si(100) surface occurs readily. The distances of the ortho-adsorbed $BCl_3$ molecule before and after optimization were markedly different, at 2.971 Å and 1.873 Å, respectively. The B atom in $BCl_3$ forms a covalent bond with the Si(100) surface and one of the B–Cl bonds is elongated, indicating that the Si atom has an attractive effect on Cl. Table 1 shows the change in distance before and after adsorption in each of the three positions.

**Table 1.** Distances before and after the adsorption of $BCl_3$ on the Si(100) surface.

| Adsorption Mode | Distance before Optimization (Å) | Optimized Distance (Å) |
| --- | --- | --- |
| Side position of the molecule | 3.191 | 2.836 |
| Lateral position of the molecule | 3.139 | 2.447 |
| Positive position of the molecule | 2.917 | 1.873 |

The adsorption energies of the three adsorption structures were then calculated. The smaller the adsorption energy, the easier it is to adsorb, and vice versa. The calculated results for the adsorption energy of the side, lateral and positive positions of the molecule are shown in Table 2.

**Table 2.** Adsorption energy of $BCl_3$ after adsorption on Si(100) surface.

| Adsorption Mode | $E_{adsorption}$ (kcal/mol) |
| --- | --- |
| Side position of the molecule | −29.2613 |
| Lateral position of the molecule | −23.5846 |
| Positive position of the molecule | −35.3549 |

According to the data in Table 2, the adsorption energies of the three adsorption modes on the Si(100) surface are all negative, indicating that $BCl_3$ molecules are readily adsorbed by the Si(100) surface and that the adsorption reaction occurs easily on the surface. The relative adsorption energies of the three molecular orientations are as follows: E (lateral position) > E (side position) > E (positive position). It can be seen that the orientation in which $BCl_3$ molecules are most easily adsorbed on the Si(100) surface is the positive position. Thus, the change in the molecular adsorption distance after adsorption was verified, and the most favorable orientation for adsorption was the positive position.

Differential electron density analysis (Figure 3a) and calculation of the charge distribution (Figure 3b) of $BCl_3$ molecules adsorbed on the Si(100) surface were also carried out. The color of the Si atoms depicted at the bridge sites on the Si(100) surface is denser, indicating that a large amount of charge is transferred in this local area and that the charge has migrated after the adsorption reaction has occurred. The B–Cl bond on the right side is clearly elongated, and an electron cloud is formed between the Cl atom and the silicon atom at the adjacent bridge site on the right, indicating that the silicon atom at the adjacent bridge site on the right has an attractive effect on the Cl atom.

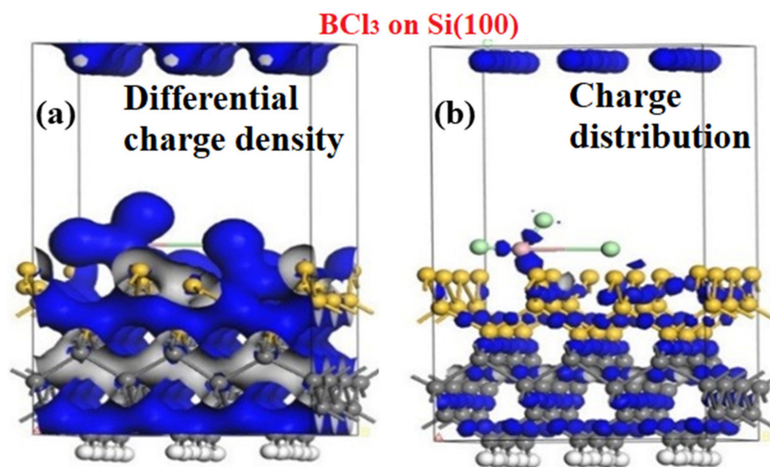


**Figure 3.** Differential charge density (**a**) and charge distribution (**b**) of $BCl_3$ adsorbed on the Si(100) surface of the unit cell.

### 3.2. Adsorption of $SiHCl_3$ Molecules on the Surface of Polysilicon Si(100)

The molecular structure of $SiHCl_3$ is tetrahedral, and we discuss here the adsorption process of optimized $SiHCl_3$ on the Si(100) surface. Figure 4 shows six possible adsorption positions on the surface, which can be described as the hydrogen top-one-positive position, hydrogen bottom-one-front position, hydrogen top-two-front position, hydrogen side-one-front position, hydrogen side-two-front position, and hydrogen bottom-two-front position. After the optimization calculation, the distance between the molecule and the surface was found to have been shortened, indicating that $SiHCl_3$ is prone to react with the surface of the Si(100) unit cell. This conclusion can also be drawn from the changes in the distance before and after adsorption at the six adsorption sites listed in Table 3. When $SiHCl_3$ is adsorbed at the second bottom-front position of the hydrogen, its distance changes from 3.000 Å to 2.340 Å. The Si atom of $SiHCl_3$ forms a covalent bond with the Si atom at the bridging position, indicating that the $SiHCl_3$ molecule has been adsorbed on the Si(100) unit cell. Simultaneously, it is observed that the Si–Cl bond of the $SiHCl_3$ molecule is distinctly elongated, which indicates that the Cl atom is attracted by the Si atom adjacent to the bridge site.

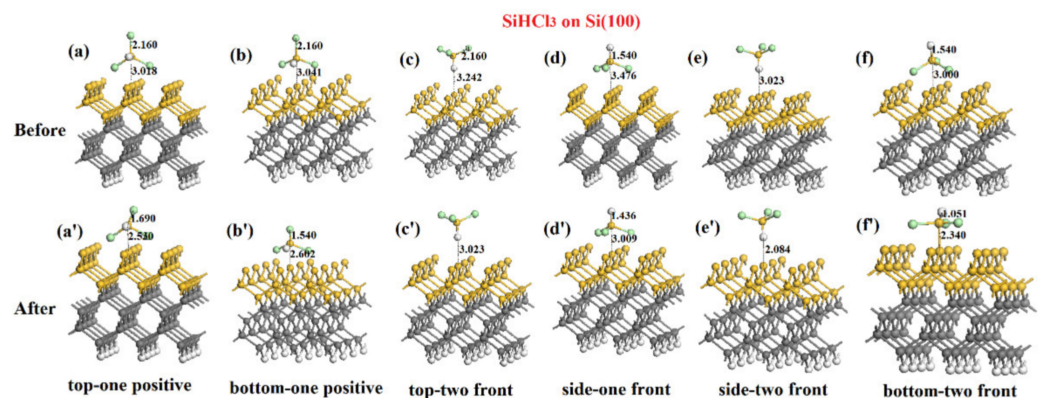


**Figure 4.** Diagram of molecular structures and distances of $SiHCl_3$ before and after adsorption on the Si(100) surface. Diagrams (**a**–**f**) show the adsorption structures before reaction, (**a′**–**f′**) those after reaction ((**a**–**f**,**a′**–**f′**) show hydrogen in the top-one-positive, bottom-one-front, top-two-front, side-one-front, side-two-front, and bottom-two-front positions, respectively).

**Table 3.** Distances before and after the adsorption of $SiHCl_3$ on the Si(100) surface.

| Adsorption Mode | Distance before Optimization (Å) | Optimized Distance (Å) |
|---|---|---|
| Hydrogen top-one-positive position | 3.018 | 2.530 |
| Hydrogen bottom-one-front position | 3.041 | 2.602 |
| Hydrogen top-two-front position | 3.242 | 3.023 |
| Hydrogen side-one-front position | 3.476 | 3.009 |
| Hydrogen side-two-front position | 3.023 | 2.804 |
| Hydrogen bottom-two-front position | 3.000 | 2.340 |

Table 4 shows the calculated adsorption energy of $SiHCl_3$ on the Si(100) surface. The adsorption energies obtained for the six adsorption structures are all negative, indicating that SiHCl3 reacts readily with the Si(100) surface. The order of the adsorption energies of the several positions is as follows: E(hydrogen side-two-front position) > E(hydrogen top-two-front position) > E(hydrogen top-one-positive position) > E(hydrogen bottom-one-front position) > E(hydrogen side-one-front position) > E(hydrogen bottom-two-front position). The adsorption energy (E) of $SiHCl_3$ is greatest when the adsorption structure of the second hydrogen base is in the front position, indicating that adsorption is more likely to occur in this orientation, at the front position of the hydrogen base 2. From the calculated adsorption energies, it can be seen that the adsorption of $SiHCl_3$ molecules in the hydrogen bottom-two-front position corresponds to the most favorable orientation, and the calculated adsorption distances confirm this conclusion.

**Table 4.** Adsorption energy of $SiHCl_3$ after adsorption on the Si(100) surface.

| Adsorption Mode | $E_{adsorption}$ (kcal/mol) |
|---|---|
| Hydrogen top-one-positive position | −4.02 |
| Hydrogen bottom-one-front position | −6.07 |
| Hydrogen top-two-front position | −3.41 |
| Hydrogen side-one-front position | −8.92 |
| Hydrogen side-two-front position | −2.47 |
| Hydrogen bottom-two-front position | −10.64 |

To gain a deeper understanding of the charge distribution in the adsorption process of $SiHCl_3$, we can use the electronic levels to characterize the reaction. The differential electron density and charge distribution of the $SiHCl_3$ molecules adsorbed on the surface of the Si(100) unit cell from the face center downward were calculated. The calculated results are shown in Figure 5a,b. From the results shown in the figure, it can be seen that the color representing the charge concentrated in the bond between the Si atoms on the Si(100) surface and the Si atom in $SiHCl_3$ is darker than that for other bonds. This not only shows that electrons have been transferred after adsorption, but also shows that a large amount of charge is transferred in this local area. Looking at the image of the adsorbed $SiHCl_3$ molecule, it is seen that the three Cl atoms and the bonding angles between the H and Si atoms in the molecule have changed, and both the Cl and H atoms show an upward posture. In addition, it can be seen that the silicon atoms on the surface and the two Si atoms at the right and back of the bridge silicon atoms adjacent to the bonded Si atoms and the corresponding Cl atoms form an electron cloud. This proves that the two have an attractive effect.

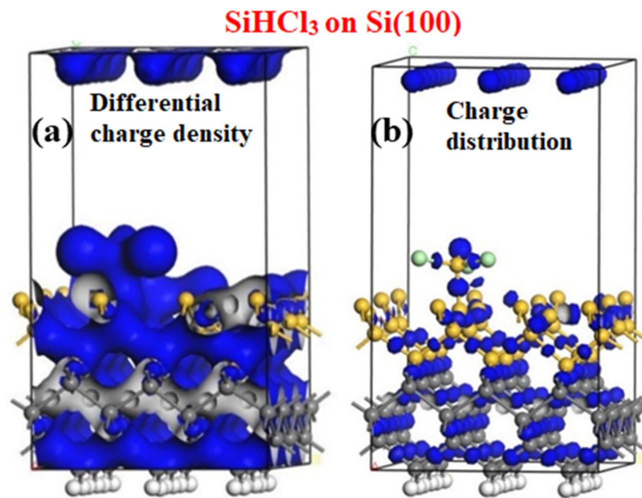


**Figure 5.** Differential charge density (**a**) and charge distribution (**b**) after $SiHCl_3$ is adsorbed on the Si(100) surface.

### *3.3. Co-Adsorption of $BCl_3$ and $SiHCl_3$ on the Surface of Polysilicon Si(100)*

A $BCl_3$ molecule and a $SiHCl_3$ molecule were placed together on the surface of the Si(100) supercell to investigate the adsorption reaction. Figure 6 shows the structural changes before and after the co-adsorption of $BCl_3$ and $SiHCl_3$ on the Si(100) surface. Compared to the structure before adsorption in Figure 6a, it can be concluded from the structure after adsorption (Figure 6b) that the Si atom in the $SiHCl_3$ molecule forms a covalent bond with the B atom in $BCl_3$. A Cl atom in each of the $BCl_3$ and $SiHCl_3$ molecules undergoes a dissociation reaction and is adsorbed on the Si atom at the nearest bridge site on the Si(100) surface. The bond lengths of the other Cl–B bonds in the $BCl_3$ molecule are significantly elongated, and the B atom is adsorbed on the Si(100) surface at the same time. These results indicate that $BCl_3$ and $SiHCl_3$ molecules are placed on the Si(100) surface simultaneously. After the adsorption reaction, it is evident that $BCl_3$ is more easily adsorbed on the Si(100) surface than is $SiHCl_3$. When $BCl_3$ and $SiHCl_3$ coexist on the Si(100) surface, they are more likely to have an effect than $SiHCl_3$ alone on the surface. Moreover, their simultaneous presence there will be accompanied by a dissociation process; in which each dissociates a Cl atom, and the Cl atom in the $BCl_3$ molecule is attracted by the Si(100) surface.

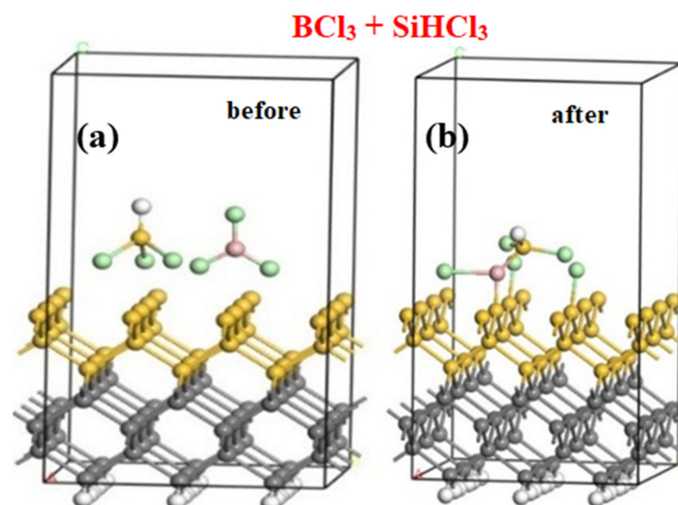


**Figure 6.** Structure changes before (**a**) and after (**b**) the co-adsorption of $BCl_3$ and $SiHCl_3$.

A microscopic electronic analysis was also performed of the charge distribution and differential electron density when $BCl_3$ and $SiHCl_3$ are present together on the surface of polysilicon. The darker blue color between $BCl_3$ and $SiHCl_3$ in Figure 7b indicates that there is a large amount of electron transfer, and it can be seen that the B–Cl bond in the $BCl_3$ molecule is distinctly elongated, and a dissociated Cl atom is adsorbed on the Si(100) surface, indicating that it charge transfer has occurred during the adsorption process. From the charge density results in Figure 7a, indicating charge transfer between the surface and the molecules, we can also see where the electrons accumulate, which proves the occurrence of the adsorption reaction.

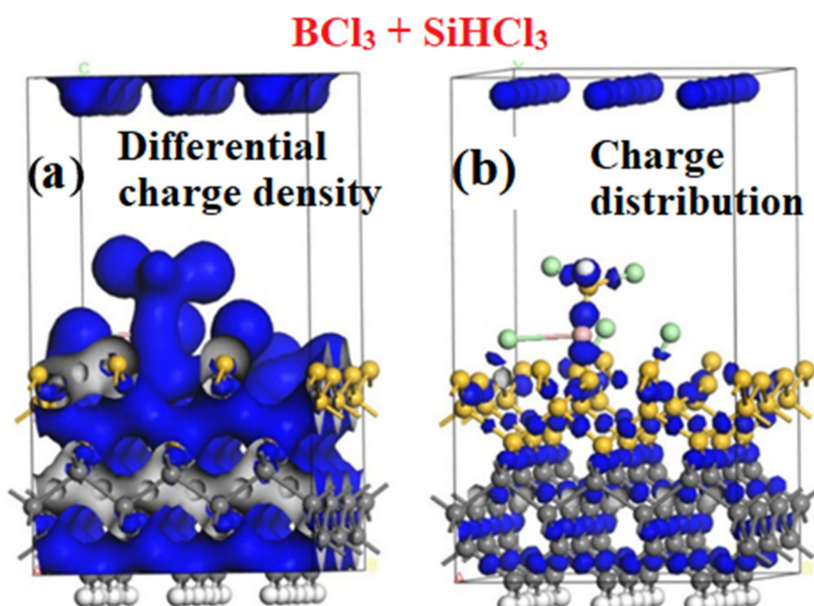


**Figure 7.** Differential charge density (**a**) and charge distribution (**b**) before and after the co-adsorption of $BCl_3$ and $SiHCl_3$ on the surface.

### *3.4. Electronic Structure Analysis*

To further understand the bonding mechanism of the adsorption of $BCl_3$ and $SiHCl_3$ on the Si(100) surface, the adsorption density of states, partial density of states, and Mulliken charge distribution were calculated, and the results are shown in Figure 8 and Table 5. It can be observed that the Si3s orbital lies far away in energy from the Fermi level on the surface of the Si(100) unit cell. After the adsorption reaction, the electrons of the Si3s orbital are not easily transferred. The valence band where electron transfer occurs is Si3p, which constitutes the valence band on the left side of the Fermi level on the surface of the Si(100) unit cell. Although it is theoretically impossible for the Si3s orbital to transfer electrons, a very small amount of electron transfer does occur from the Si3s orbital after the reaction. The valence state on the right side of the Fermi level is composed of Si3d orbitals, and the bandgap between the top of the valence band and the bottom of the conduction band is 1.502 eV. After the reaction, the bandgap is reduced to 0.087 eV. The narrowing of the bandgap indicates that the Si is more likely to react, and its chemical properties become more active, which in turn indicates that it is more likely to interact with $BCl_3$ and $SiHCl_3$ molecules.

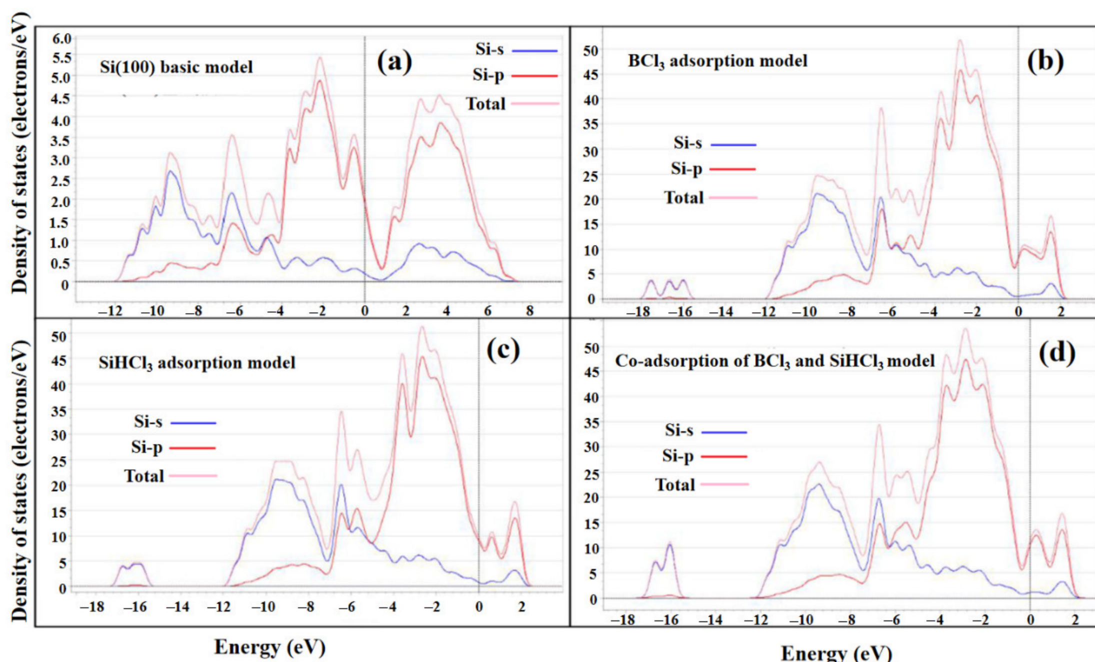


**Figure 8.** State density changes of $BCl_3$ and $SiHCl_3$ molecules after the adsorption on the Si(100) cell surface. (**a**) is the density of states of Si(100); (**b**) is the density of states for the $BCl_3$ adsorption model; (**c**) is the density of states for the $SiHCl_3$ adsorption model; (**d**) is the density of states for the co-adsorption of $BCl_3$ and $SiHCl_3$.

**Table 5.** Mulliken charge co-adsorption of $BCl_3$ and $SiHCl_3$ molecules on the surface of Si(100) unit cell.

| Project | Species | S | p | d | Total | Charge (eV) | Change (eV) |
|---|---|---|---|---|---|---|---|
| Ideal $BCl_3$ | B | 0 | 6.26 | 2.44 | 10.87 | 1.13 | 0 |
| | Cl1 | 1.96 | 5.33 | 0 | 7.28 | −0.28 | |
| | Cl2 | 1.96 | 5.33 | 0 | 7.28 | −0.28 | |
| | Cl3 | 1.96 | 5.32 | 0 | 7.28 | −0.28 | |
| Ideal $SiHCl_3$ | Si | 3.18 | 7.42 | 3.36 | 13.96 | 1.13 | 0 |
| | Cl1 | 2.08 | 6.12 | 0 | 8.20 | −0.32 | |
| | Cl2 | 2.08 | 6.12 | 0 | 8.20 | −0.33 | |
| | Cl3 | 2.08 | 6.12 | 0 | 8.20 | −0.35 | |
| | H | 1.76 | 4.28 | 0 | 6.04 | −0.30 | |
| Si(100) surface adsorption $BCl_3$ | B | 0 | 6.23 | 2.17 | 10.68 | 1.32 | 0.29 |
| | Cl1 | 1.95 | 5.36 | 0 | 7.34 | −0.31 | |
| | Cl2 | 1.95 | 5.32 | 0 | 7.27 | −0.27 | |
| | Cl3 | 1.95 | 5.33 | 0 | 7.28 | −0.28 | |
| Si(100) surface adsorption $SiHCl_3$ | Si | 2.21 | 6.14 | 2.13 | 10.48 | 1.02 | 0.24 |
| | Cl1 | 1.95 | 5.39 | 0 | 7.34 | −0.34 | |
| | Cl2 | 1.95 | 5.39 | 0 | 7.24 | −0.34 | |
| | Cl3 | 1.95 | 5.33 | 0 | 7.29 | −0.29 | |
| | H | 1.95 | 5.36 | 0 | 7.34 | −0.31 | |

By analyzing the electronic density of states of $BCl_3$ and $SiHCl_3$ molecules adsorbed on the surface of the Si(100) unit cell in Figure 8, it is found that after the two molecules are adsorbed on the surface of the unit cell, their band gaps are narrowed and the electrons inside the molecules are transferred to the outermost electron layer and to the conduction band, which is more reactive. Based on molecular chemical structure theory, we know that the B atom in the $BCl_3$ molecule has three coordination sites, and the electron configuration of B is $1s^2 2s^2 2p^1$, showing that B is an electron deficient atom. Six electrons are provided

by three Cl atoms, and each of the three Cl atoms also provides a filled 2p orbital that is side-by-side with an empty p orbital of the B atom and is thus able to form a strong π bond. The formation of bonds by $sp^2$ hybridization can explain the three B–Cl bonds in $BCl_3$. Similarly, for the $SiHCl_3$ molecule, electrons are transferred to the outermost electron layer. The Si atom in the $SiHCl_3$ molecule has four coordination sites and the outermost electron configuration is $3s^2 3p^2$, which is eventually completed by the four covalent bonds formed with Si. This can explain the origin of the four covalent bonds, and it can be concluded that the spatial configuration of $SiHCl_3$ is a that of a regular tetrahedron.

From the Mulliken charge distribution of the two molecules shown in Table 5, it can be observed that when $SiHCl_3$ is adsorbed on the surface of the Si(100) unit cell, charge transfer occurs, and there are two charge transfer paths. The first is the transfer of 1.30 eV of charge from the Si atom of the $SiHCl_3$ molecule to the surface of the unit cell. The second is charge transfer from the surface of the unit cell to the three Cl atoms and the H atom of the $SiHCl_3$ molecule, a charge transfer of 1.06 eV. After fitting and offsetting, it is found that during the entire adsorption reaction of $SiHCl_3$ on the surface of the Si(100) unit cell, the Si atom in the $SiHCl_3$ has transferred a net 0.24 eV of charge to the surface of the Si(100) unit cell. When $BCl_3$ is adsorbed on the surface of the Si(100) unit cell, significant charge transfer also occurs, and there are two charge transfer paths. The first is a transfer of 1.52 eV from the B atom in $BCl_3$ to the surface of the unit cell. The second is a transfer of 1.23 eV from the surface of the unit cell to the three Cl atoms and one H atom in the $BCl_3$ molecule. After fitting and offsetting, during the entire adsorption reaction of $BCl_3$ on the surface of the Si(100) unit cell, the B atom in $BCl_3$ is seen to have transferred 0.29 eV of charge to the surface of the Si(100) unit cell.

According to the results for transfer of electrons between $SiHCl_3$, $BCl_3$, and the surface of polysilicon during the adsorption process, both molecules transfer charge to the surface of the unit cell during adsorption, with $BCl_3$ transferring 0.05 eV more charge to the surface of the Si(100) unit cell than $SiHCl_3$ does. It can be shown that the surface of the Si(100) unit cell has a definite adsorption effect on $BCl_3$ and $SiHCl_3$ molecules, and that the B atoms in $BCl_3$ are more easily adsorbed on the Si(100) surface, which means that B and polysilicon will be deposited on the silicon rod together during the production process. The above results also explain the phenomenon that when $BCl_3$ and $SiHCl_3$ molecules are co-adsorbed on the surface of the Si(100) unit cell, the Si atoms in the $SiHCl_3$ molecules first form a covalent bond with the B atoms in $BCl_3$.

The B impurities may deposit on the surface of the silicon rod competing with polysilicon and the trace B-compound impurities may be enriched by the influence of transport phenomena. The above two phenomena are the main reasons causing the high-impurity B in the silicon production. It is obvious that the adsorption of $BCl_3$ on silicon to cause the deposition of B on silicon surface. Therefore, transport phenomenon investigation may be effective method to reduce boron impurity inside poly-silicon, such as increasing mole fraction of $H_2$ and temperature.

## 4. Conclusions

(1) $BCl_3$ and $SiHCl_3$ are mainly adsorbed on the surface of the Si(100) unit cell in the positive position and the hydrogen bottom-two-front position of the molecule, respectively. The discrete distances of $BCl_3$ and $SiHCl_3$ from the surface of the Si(100) unit cell are 1.873 Å and 2.340 Å, respectively, and the separation energies are −35.2549 kcal/mol and −10.64 kcal/mol, respectively.

(2) Compared with $SiHCl_3$, $BCl_3$ reacts more easily with the Si(100) surface, and when $BCl_3$ and $SiHCl_3$ coexist, $BCl_3$ reacts more readily than $SiHCl_3$ with the Si(100) surface. When $BCl_3$ and $SiHCl_3$ are present simultaneously, the gas phase reaction is accompanied by a dissociation process, in which each molecule dissociates a Cl atom that is adsorbed on the Si(100) surface. At the same time, a distinctly elongated B–Cl bond shows that the Si(100) surface also has an attractive effect on Cl atoms.

(3) After the adsorption of $SiHCl_3$ and $BCl_3$, 0.24 and 0.29 eV of charge, respectively, are found to have been transferred from the molecule to the surface of the unit cell. Both $BCl_3$ and $SiHCl_3$ are readily adsorbed on the surface of the Si(100) unit cell, but $BCl_3$ is more easily adsorbed. These results confirm that the B atom in $BCl_3$ in the adsorption model forms a covalent bond with the Si atom on the Si(100) unit cell surface, and the Si atom in the $SiHCl_3$ molecule forms a covalent bond with the B atom in $BCl_3$.

**Author Contributions:** Conceptualization, L.H. and Y.H.; Data curation, F.C., Y.H. and N.Y.; Investigation, J.W., Y.H. and N.Y.; Methodology, N.Y. and G.X.; Software, L.T. and L.H.; Validation, Q.Y.; Writing—Original draft, Q.Y.; Writing—Review and editing, Q.Y., J.W. and Y.H. All authors have read and agreed to the published version of the manuscript.

**Funding:** This research was funded by the National Natural Science Foundation of China Project (No. 21566015 and No. 52074141).

**Institutional Review Board Statement:** Not applicable.

**Informed Consent Statement:** Informed consent was obtained from all subjects involved in the study.

**Data Availability Statement:** Data sharing not applicable. No new data were created or analyzed in this study. Data sharing is not applicable to this article.

**Conflicts of Interest:** The authors declare no conflict of interest.

## References

1. Chen, J.; Zhang, X. Prediction of thermal conductivity and phonon spectral of silicon material with pores for semiconductor device. *Phys. B Condens. Matter* **2021**, *614*, 413034. [CrossRef]
2. Chen, P.; Zeng, Q.; Guo, W.; Chen, J. The source, enrichment and precipitation of ore-forming elements for porphyry Mo deposit: Evidences from melt inclusions, biotite and fluorite in Dasuji deposit, China. *Ore Geol. Rev.* **2021**, *135*, 104205. [CrossRef]
3. Cheng, D.; Gao, Y.; Liu, R. Finite element analysis on processing stress of polysilicon cut by diamond multi-wire saw. *Mater. Sci. Semicond. Process.* **2021**, *131*, 105860. [CrossRef]
4. Xiong, Q.M.; Chen, Z.; Huang, J.-T.; Zhang, M.; Song, H.; Hou, X.F.; Li, X.B.; Feng, Z.J. Preparation, structure and mechanical properties of Sialon ceramics by transition metal-catalyzed nitriding reaction. *Rare Met.* **2020**, *39*, 589–596. [CrossRef]
5. Zhou, L.; Li, S.; Tang, Q.; Deng, X.; Wei, K.; Ma, W. Effects of solidification rate on the leaching behavior of metallic impurities in metallurgical grade silicon. *J. Alloys Compd.* **2021**, *882*, 160570. [CrossRef]
6. Gao, M.; Liu, B.; Zhang, X.; Zhang, Y.; Li, X.; Han, G. Ultrathin $MoS_2$ nanosheets anchored on carbon nanofibers as free-standing flexible anode with stable lithium storage performance. *J. Alloys Compd.* **2022**, *894*, 162550. [CrossRef]
7. O'Mara, W.; Herring, R.B.; Hunt, L.P. *Handbook of Semiconductor Silicon Technology*; Crest Publishing House: Kettering, UK, 2007.
8. Davis, K.O.; Brooker, R.P.; Seigneur, H.P.; Rodgers, M.; Rudack, A.C.; Schoenfeld, W.V. Pareto analysis of critical challenges for emerging manufacturing technologies in silicon photovoltaics. *Sol. Energy* **2014**, *107*, 681–691. [CrossRef]
9. Chanlaor, P.; Limtrakul, S.; Vatanatham, T.; Ramachandran, P.A. Modeling of Chemical Vapor Deposition of Silane for Silicon Production in a Spouted Bed via Discrete Element Method Coupled with Eulerian Model. *Ind. Eng. Chem. Res.* **2018**, *57*, 12096–12112. [CrossRef]
10. Filtvedt, W.O.; Holt, A.; Ramachandran, P.A.; Melaaen, M.C. Chemical vapor deposition of silicon from silane: Review of growth mechanisms and modeling/scaleup of fluidized bed reactors. *Sol. Energy Mater. Sol. Cells* **2012**, *107*, 188–200. [CrossRef]
11. Shi, S.; Guo, X.; An, G.; Jiang, D.; Qin, S.; Meng, J.; Li, P.; Tan, Y.; Noor ul Huda Khan Asghar, H.M. Separation of boron from silicon by steam-added electron beam melting. *Sep. Purif. Technol.* **2019**, *215*, 242–248. [CrossRef]
12. Wang, C.; Wang, T.; Li, P.; Wang, Z. Recycling of $SiCl_4$ in the manufacture of granular polysilicon in a fluidized bed reactor. *Chem. Eng. J.* **2013**, *220*, 81–88. [CrossRef]
13. Safarian, J. Thermochemical Aspects of Boron and Phosphorus Distribution Between Silicon and BaO-$SiO_2$ and CaO-BaO-$SiO_2$ lags. *Silicon* **2019**, *11*, 437–451. [CrossRef]
14. Bye, G.; Ceccaroli, B. Solar grade silicon: Technology status and industrial trends. *Sol. Energy Mater. Sol. Cells* **2014**, *130*, 634–646. [CrossRef]
15. Bullón, J.; Margaria, T.; Miranda, A.; Mıguez, J. Physical and chemical analysis of the upgraded metallurgical silicon for the solar industry. In *Silicon Form the Chemical and Solar Industry IX*; Norwegian University of Science and Technology: Oslo, Norway, 2008.
16. Haupfear, E.A.; Schmidt, L.D. Kinetics of boron deposition from $BBR_3$ + $H_2$. *Chem. Eng. Sci.* **1994**, *49*, 2467–2481. [CrossRef]
17. Liu, W.; Huang, F.; Liao, Y.; Zhang, J.; Ren, G.; Zhuang, Z.; Zhen, J.; Lin, Z.; Wang, C. Treatment of CrVI-Containing $Mg(OH)_2$ Nanowaste. *Angew. Chem.* **2008**, *120*, 5701–5704. [CrossRef]

18. Jenkinson, J.P.; Pollard, R. Thermal diffusion effects in chemical vapor deposition reactors. *J. Electrochem. Soc.* **1984**, *131*, 2911. [CrossRef]
19. Sezgi, N.A.; Ersoy, A.; Dogu, T.; Özbelge, H.Ö. CVD of boron and dichloroborane formation in a hot-wire fiber growth reactor. *Chem. Eng. Process. Process Intensif.* **2001**, *40*, 525–530. [CrossRef]
20. Asli Sezgi, N.; Dogu, T.; Onder Ozbelge, H. Mechanism of CVD of boron by hydrogen reduction of $BCl_3$ in a dual impinging-jet reactor. *Chem. Eng. Sci.* **1999**, *54*, 3297–3304. [CrossRef]
21. Liu, Y.; Zhang, L.; Cheng, L.; Zeng, Q.; Zhang, W.; Yang, W.; Feng, Z.; Li, S.; Zeng, B. Uniform design and regression analysis of LPCVD boron carbide from $BCl_3$–$CH_4$–$H_2$ system. *Appl. Surf. Sci.* **2009**, *255*, 5729–5735. [CrossRef]
22. Deng, J.; Cheng, L.; Zheng, G.; Su, K.; Zhang, L. Thermodynamic study on co-deposition of $ZrB_2$–SiC from $ZrCl_4$–$BCl_3$–$CH_3SiCl_3$–$H_2$–Ar system. *Thin Solid Film.* **2012**, *520*, 7030–7034. [CrossRef]
23. Mahammedi, N.A.; Ferhat, M.; Belkada, R. Prediction of indirect to direct band gap transition under tensile biaxial strain in type-I guest-free silicon clathrate Si46: A first-principles approach. *Superlattices Microstruct.* **2016**, *100*, 296–305. [CrossRef]
24. Delley, B. An all-electron numerical method for solving the local density functional for polyatomic molecules. *J. Chem. Phys.* **1990**, *92*, 508–517. [CrossRef]
25. Clark, S.J.; Segall, M.D.; Pickard, C.J.; Hasnip, P.J.; Probert, M.I.; Refson, K.; Payne, M.C. First principles methods using CASTEP. *Z. Für Krist. Cryst. Mater.* **2005**, *220*, 567–570. [CrossRef]
26. Zhang, Y.F.; Viñes, F.; Xu, Y.J.; Li, Y.; Li, J.Q.; Illas, F. Role of Kinetics in the Selective Surface Oxidations of Transition Metal Carbides. *J. Phys. Chem. B* **2006**, *110*, 15454–15458. [CrossRef] [PubMed]
27. Vanderbilt, D. Soft self-consistent pseudopotentials in a generalized eigenvalue formalism. *Phys. Rev. B* **1990**, *41*, 7892. [CrossRef] [PubMed]
28. Wang, Z.; Chen, X.; Cheng, Y.; Niu, C. Adsorption and Deposition of $Li_2O_2$ on the Pristine and Oxidized TiC Surface by First-principles Calculation. *J. Phys. Chem. C* **2015**, *119*, 25684–25695. [CrossRef]
29. Sun, W.; Ceder, G. Efficient creation and convergence of surface slabs. *Surf. Sci.* **2013**, *617*, 53–59. [CrossRef]
30. Peng, M.; Shi, B.; Han, Y.; Li, W.; Zhang, J. Crystal facet dependence of SiHCl3 reduction to Si mechanism on silicon rod. *Appl. Surf. Sci.* **2022**, *580*, 152366. [CrossRef]
31. Galán, O.A.L.; Carbajal-Franco, G. Energy profiles by DFT methods for CO and NO catalytic adsorption over ZnO surfaces. *Catal. Today* **2021**, *360*, 38–45. [CrossRef]